BIOCHEMISTRY
including biophysical chemistry & molecular biology

Article

pubs.acs.org/biochemistry

# Oxidative Uncoupling in Cysteine Dioxygenase Is Gated by a Proton-Sensitive Intermediate

Joshua K. Crowell, Wei Li, and Brad S. Pierce*

Department of Chemistry and Biochemistry, College of Sciences, The University of Texas at Arlington, Arlington, Texas 76019, United States

Supporting Information

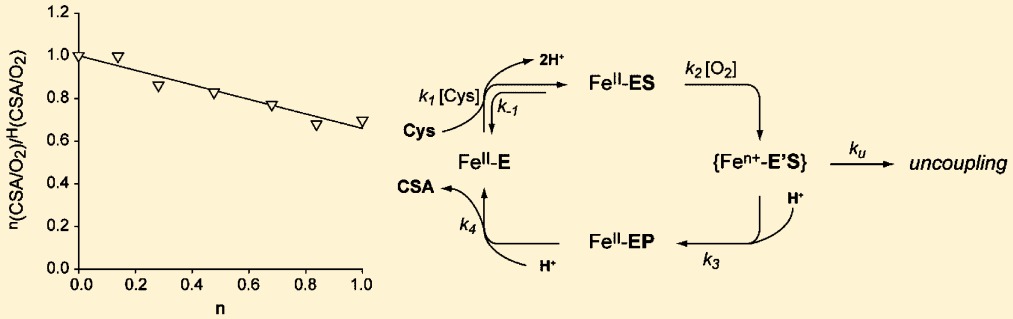


**ABSTRACT:** Cysteine dioxygenase (CDO) is a non-heme mononuclear iron enzyme that catalyzes the $O_2$-dependent oxidation of L-cysteine (Cys) to produce cysteine sulfinic acid (CSA). This enzyme catalyzes the first committed step in Cys catabolism; thus, it is central to mammalian sulfur metabolism and redox homeostasis. Ironically, despite nearly 45 years of continued research on CDO, essentially no information has been reported with respect to its kinetic mechanism. In this work, the timing of chemical steps in the CDO kinetic mechanism is investigated by pH/pD-dependent steady-state kinetics and solvent isotope effects on $k_{cat}$, $k_{cat}/K_M$, and $(O_2/CSA)$ coupling. Normal solvent kinetic isotope effects of 1.45 ± 0.05 and 2.0 ± 0.1 are observed in $k_{cat}$−pL and $k_{cat}/K_M$−pL profiles, respectively. Proton inventory experiments within the pL-independent region (pL 8.5) suggest multiple solvent-exchangeable protons in flight for both $k_{cat}$ and $k_{cat}/K_M$ data. The influence of solvent viscosity was also investigated to probe non-chemical steps and to verify that the apparent isotope effects were not attributable to increased solvent viscosity of $D_2O$ reactions relative to $H_2O$. Although solvent viscosity did have a modest influence on $k_{cat}$ and $k_{cat}/K_M$, the response is not sufficient to account for the observed solvent isotope effects. This suggests that product release is only partially rate-limiting for CDO catalysis. Most crucially, proton inventory of $(O_2/CSA)$ coupling indicates that a proton-sensitive transition state directly follows $O_2$ activation. Thus, protonation of a transient species preceding Cys oxidation is gated by protons in flight. This behavior provides valuable insight into the kinetically masked transients generated during catalysis.

Thiol dioxygenase (TDO) enzymes utilize a monouclear ferrous iron active site to catalyze the $O_2$-dependent oxidation of sulfur-containing amino acid derivatives without need for an external electron source. The only known TDO enzymes identified in mammals are cysteine dioxygenase (CDO) and cysteamine (2-aminoethanethiol) dioxygenase (ADO).[1] Between these enzymes, CDO is the most extensively characterized. This enzyme catalyzes the first irreversible step in the catabolic pathway of L-cysteine (Cys) to produce cysteine sulfinic acid (CSA).[2] CDO has been of considerable interest recently, as enzymes involved in sulfur oxidation and transfer are increasingly being recognized as potential drug targets for development of antimicrobials and therapies for cancer and inflammatory disease.[3−6]

CDO belongs to the mononuclear non-heme iron family of enzymes. Non-heme mononuclear iron enzymes exhibit remarkable versatility in the chemical oxidations they catalyze. As with most oxidase and oxygenase enzymes, $O_2$ reactivity in CDO is gated by substrate binding.[7] This obligate-ordered addition of Cys substrate prior to $O_2$ facilitates high catalytic efficiency and limits self-oxidation. Currently, the exact mechanism by which oxidase and oxygenase enzymes couple substrate binding to trigger reactivity with molecular oxygen is not well understood.

As shown in Figure 1A, the mononuclear ferrous iron site within resting CDO is coordinated by the Nε-atoms of His86, His88, and His140.[8−10] This active site coordination represents a significant departure from the canonical 2-His-1-carboxylate facial triad observed in nearly all other members of this enzyme family.[11] Indeed, only two other crystallographically characterized non-heme mononuclear iron enzymes exhibit a similar 3-His Fe-site coordination [gentisate 1,2-dioxygenase (GDO); diketone dioxygenase (Dke1)].[12,13]

**Received:** October 1, 2014
**Revised:** November 10, 2014
**Published:** November 11, 2014





dx.doi.org/10.1021/bi501241d | *Biochemistry* 2014, 53, 7541−7548

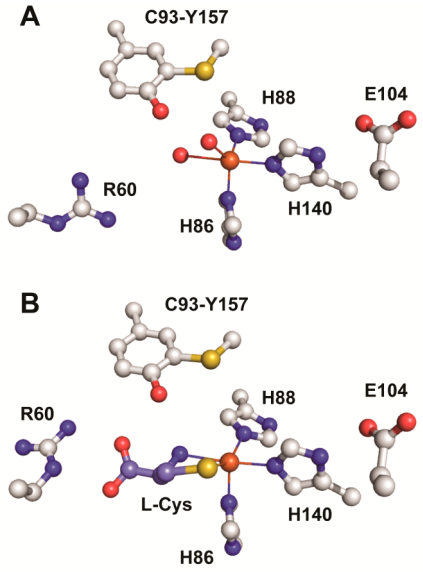


**Figure 1.** 1.6 Å resolution crystal structures for the resting (A) (PDB code 4IEZ) and substrate-bound (B) (PDB code 4IEV) mammalian CDO active site at pH 8.0.[10]

Another unusual feature within the active site of eukaryotic CDO enzymes is a covalently cross-linked cysteine−tyrosine (C93−Y157) pair. This post-translational modification is located 3.3 Å from the mononuclear iron site.[9] Interestingly, among CDO enzymes identified across phylogenic domains, only the Y157 residue is conserved. Thus, the C93−Y157 pair is unique to eukaryotic enzymes. In principle, this post-translational modification could simply be the result of self-oxidation due to enzymatic uncoupling. For instance, analogous self-hydroxylation events have been reported for the non-heme mononuclear iron enzymes taurine dioxygense, prolyl-4-hydroxylase, and lysyl hydroxylase.[14−18] However, unlike these enzymes, which are inactivated over multiple catalytic turnovers, several reports have demonstrated that formation of the C93−Y157 cross-link in CDO actually increases catalytic activity, specificity, and ($O_2$/CSA)-coupling efficiency.[19−21] Therefore, although the exact role of this modification is not yet fully understood, it does appear to have a positive impact on *in vitro* catalysis.

To date, CDO has been extensively studied crystallographically,[8−10] spectroscopically (EPR, Mössbauer, CD/MCD),[22−25] and mechanistically.[26−28] Despite these studies, no information is currently available regarding the relative timing of chemical and non-chemical steps during CDO-catalyzed reactions. The development of a kinetic mechanism for CDO is invaluable for evaluating the validity of chemical steps proposed within the enzymatic catalytic cycle. For this purpose, the influence of pH, solvent isotope, and viscosity effects was monitored for CDO steady-state kinetic parameters ($k_{cat}$ and $k_{cat}/K_M$). Proton inventory experiments were performed to monitor the number of exchangeable protons in flight during chemical steps. The timing of non-chemical steps was investigated by measuring the influence of solvent viscosity on enzyme kinetics. One key finding demonstrated by these studies is that ($O_2$/CSA) coupling of CDO exhibits a normal solvent isotope effect of 1.45 ± 0.05. This observation suggests that a proton-sensitive transition state immediately precedes Cys oxidation in CDO-catalyzed reactions. This behavior has been observed for other non-heme mononuclear iron enzymes and thus provides insight into the nature of transient intermediates generated during CDO catalysis.[29−31]

## MATERIALS AND METHODS

**Purification.** Recombinant *Mus musculus* CDO [EC 1.13.11.20] was expressed and purified as described previously.[21,28] Conversion of CDO to the fully modified enzyme containing stoichiometric C93−Y157 cross-link was performed using a modified version of the published method.[21] Briefly, following cleavage from maltose binding protein (MBP) by tobacco etch virus protease (TEV), the isolated enzyme (typically ∼35 μmol) was added to a solution 400 mL of 10 mM HEPES, 100 mM NaCl, and 20 mM L-cysteine and allowed to gently mix by magnetic stir bar for 45 min at 37 °C. The resulting enzyme was concentrated using an Amicon $N_2$ stirred cell equipped with an YM-10 ultrafiltration membrane (Millapore) to a final volume of ∼10 mL. Enzyme solutions were exchanged into the storage buffer (10 mM HEPES, 300 mM NaCl, pH 7.5) by overnight dialysis (Spectra/Por). Remaining MBP and trace TEV protease were removed by subtractive IMAC (GE Healthcare, IMAC Sepharose) as described elsewhere. The concentration of CDO protein was determined using the published extinction coefficient at 280 nm (28 300 $M^{-1}$ $cm^{-1}$). The ferrous and ferric iron content within CDO was assayed spectrophotometrically for all batches of enzyme used in these experiments as described previously.[25] For clarity, the concentrations reported in enzymatic assays reflect the concentration of ferrous iron within samples of CDO ($Fe^{II}$−CDO). Verification of stoichiometric C93−Y157 cross-link formation in CDO was confirmed by SDS-PAGE and densitometry. The specific activity and Fe content of CDO utilized in these experiments was comparable to those observed previously.

**Enzyme Assays.** Cysteine sulfinic acid (CSA) was assayed using the HPLC method described previously.[21,25] In a typical 1 mL reaction mixture, a stock solution of freshly prepared Cys was added to a buffered solution (10 mM HEPES, 50 mM NaCl, pH 8.5) to obtain a final concentration of 0.1−20 mM Cys. Each reaction vial was held at constant temperature (20 ± 2 °C), and the reaction was initiated by addition of CDO (typically 0.5−1.0 μM). Sample aliquots (250 μL) were removed from the reaction vial at selected time points (1, 2, and 3 min) and quenched by addition of 10 μL of 1 N HCl (final pH 2.0) followed by spin-filtration (0.22 μm cellulose acetate membrane; Corning, Spin-X) prior to HPLC analysis. The concentration of CSA produced was determined by comparison to calibration curves ranging from (0.1−5 mM CSA). The rate of dioxygen consumption in CDO activity assays was determined using a standard Clark electrode (Hansatech Instruments, Norfolk, England) in a jacketed 2.5 mL cell. As with HPLC assays, reaction temperatures were maintained at 20 ± 2 °C by a circulating water bath (ThermoFlex 900, Thermo Scientific).

All reaction mixtures used in steady-state experiments where $O_2$ content was varied were prepared anaerobically on a Schlenk line prior to transferring into the anaerobic chamber (Coy Laboratory Products Inc., Grass City, MI). The Schlenk line is equipped with analytical grade argon gas passed through a copper catalyst (Kontes, Vineland, NJ) to remove trace $O_2$ impurities. Desired oxygen concentrations were prepared by mixing anaerobic reaction mixtures with an $O_2$-saturated buffer prepared by sparging $O_2$ gas into the reaction buffer for 20 min under constant stirring (20 ± 2 °C). Reaction mixtures (2 mL)


dx.doi.org/10.1021/bi501241d | *Biochemistry* 2014, 53, 7541−7548

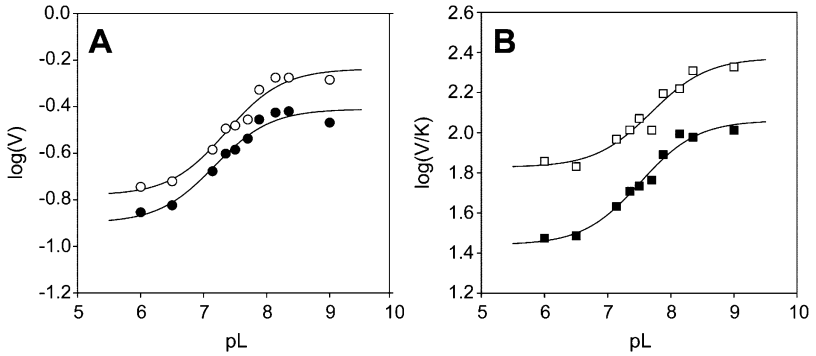


**Figure 2.** pL dependence of steady-state kinetic parameters of cysteine dioxygenase with L-cysteine as a substrate. Both log($V$) and log($V/K$) pL profiles were fit to eq 1. The p$K_a$ values determined from log($V$) fits were 7.42 ± 0.12 ($H_2O$, ○) and 7.63 ± 0.11 ($D_2O$, ●). The p$K_a$ values obtained from log($V/K$) fits were 7.96 ± 0.17 ($H_2O$, □) and 7.82 ± 0.14 ($D_2O$, ■). The observed solvent isotope effect for CDO at pH 8.5/pD 8.9 for $V$ and $V/K$ is 1.45 ± 0.05 and 2.0 ± 0.1, respectively.

were prepared with final $O_2$ concentrations ranging from 50−300 μM and a fixed Cys concentration of 20 mM.

**Solvent Isotope Effects.** For pL profiles and solvent isotope studies, the buffer components were prepared directly in $D_2O$ and adjusted by direct addition of NaOD or DCl. pD values were obtained from the pH electrode reading using the relationship pD = pH + 0.4.[32−34] The composition of reaction buffers for all pH/D profile experiments consisted of 10 mM Good's buffer and 50 mM NaCl. 2-(*N*-Morpholino)-ethanesulfonic acid (MES) was used to buffer reactions over the pH/D range of 6.0−6.9 and 2-[4-(2-hydroxyethyl)-piperazin-1-yl]ethanesulfonic acid (HEPES) was used to buffer reactions over the pH/D range of 7.0−8.5. 2-(Cyclohexylamino)ethanesulfonic acid (CHES) was used to buffer reactions over the pH/D range of 8.5−10. Although activity measurements were made above pH/D 9.0, the results were highly variable, and obvious signs of protein aggregation were observed. For this reason, only results obtained between pH/D values of 6 to 9 are presented. For proton inventory experiments, the mole fraction of $D_2O$ ($n$) was calculated on the basis of combining appropriate ratios of buffer prepared in $D_2O$ and $H_2O$. Steady-state kinetic parameters ($k_{cat}$ and $k_{cat}/K_M$) were obtained by measuring both $O_2$ consumption and CSA formation at varying mole fractions of $D_2O$ (pL 8.5).

**Viscosity Studies.** For solvent viscosity studies, the steady-state kinetic parameters ($k_{cat}$ and $k_{cat}/K_M$) were determined for CDO catalysis using both oxygen electrode and HPLC at pH 8.5 (20 °C) as described above. Sucrose and glycerol were utilized as viscosigens to increase the buffer viscosity within CDO reaction mixtures. The viscosity ($\eta$) of buffers containing sucrose and glycerol was measured using an Ostwald viscometer relative to 10 mM HEPES, pH 8.5 (20 °C). The values obtained represent the average of triplicate measurements. In these experiments, addition of glycerol up to 33% (w/w) was used to increase the relative viscosity of the buffer ($\eta_{rel}$) up to 3-times that of the control buffer. Addition of up to 35% sucrose (w/v) was used to accomplish a similar increase in the relative viscosity of reaction buffers.

**Data Analysis.** Steady-state kinetic parameters for CDO were determined by fitting data to the Michaelis−Menten equation using the program SigmaPlot, ver. 11.0 (Systat Software Inc., Chicago, IL). The pH/D-dependences of steady-state kinetic parameters ($k_{cat}$ or $k_{cat}/K_M$) for CDO approaches limiting values ($Y_L$ and $Y_H$) at low and high pH and thus data were fit to eq 1.[35,36] Here, [H] and $K_1$ represent the hydrogen ion (or deuterium ion) concentration and dissociation constant for ionizable groups involved in catalysis, respectively.

$$\log Y = \log\left(\frac{Y_L + Y_H \cdot \frac{K_1}{[H]}}{1 + \frac{K_1}{[H]}}\right) \quad (1)$$

Equation 2 was used to fit $k_{cat}$ and $k_{cat}/K_M$ proton inventory data for CDO.[37] In this equation, $n$ is the mole fraction of $D_2O$ present in reaction buffer and $E_0$ and $E_n$ are the $k_{cat}$ or $k_{cat}/K_M$ values in $H_2O$ and at the specific mole fraction of $D_2O$, respectively.[33,34] The measured solvent kinetic isotope effect is designated by KIE. The integer value ($y$) describes the number of protons ($y$ = 1, 2, ...) with equivalent fractionation factors that contribute to the isotope effect.

$$\frac{E_n}{E_0} = \left(1 - n + \left(\frac{n}{KIE}\right)\right)^y \quad (2)$$

Proton inventory of enzymatic coupling results were fit to eq 3 as described previously.[38] Here, the microscopic rate constants for productive and unproductive catalysis are designated by $k_p$ and $k_u$, respectively. The coupling efficiency ($C$) is defined by the mol of CSA produced per mol of $O_2$ consumed. At each mole fraction $D_2O$ ($n$), coupling values ($^nC$) were normalized by the value observed in $H_2O$ reactions ($^HC$). The solvent kinetic isotope effect on enzymatic coupling is designated by KIE ($^{D_2O}k = k_{obs}^{H_2O}/k_{obs}^{D_2O}$).

$$^DC = \frac{1 - n + (n/KIE) + k_p/k_u}{1 + k_p/k_u} \quad (3)$$

The influence of solvent viscosity on steady-state parameters ($k_{cat}$ and $k_{cat}/K_M$) was fit to eq 4. In these experiments, $Y_0$ is the $k_{cat}$ or $k_{cat}/K_M$ determined in the absence of any viscosigen, $Y_\eta$ is the values observed at each specific viscosity, $\eta_{rel}$ is the viscosity relative to 10 mM HEPES, pH 8.5, at 20 °C, and $m$ is the slope of the line that indicates the extent of diffusion limitation. The relative viscosities of buffered solutions were determined as described above.

$$\frac{Y_0}{Y_\eta} = 1 + m \cdot \eta_{rel} \quad (4)$$


dx.doi.org/10.1021/bi501241d | *Biochemistry* 2014, 53, 7541−7548

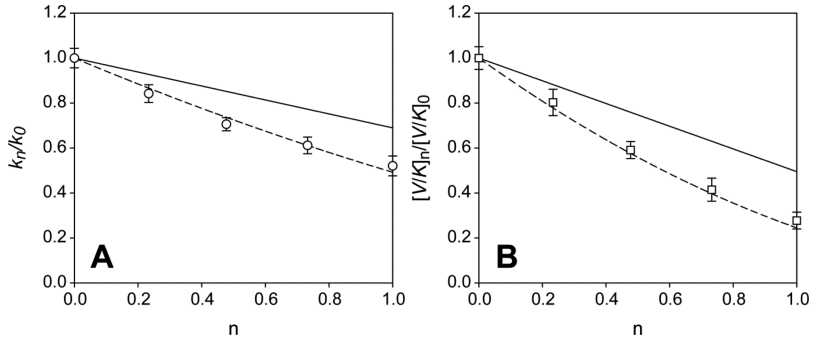


**Figure 3.** Proton inventory of CDO catalyzed formation at pL 8.5. Plot of normalized V ($k_n/k_0$; top) and $V/K$ ($[V/K]_n/[V/K]_0$; bottom) versus mole fraction $D_2O$. Experimentally determined SKIE values for $k_{cat}$ and $k_{cat}/K_M$ were used to fit data to eq 2. For both $k_n/k_0$ and $[V/K]_i/[V/K]_0$, proton inventory fits assuming a single proton in flight (solid line, $y = 1$) did not converge. Significantly better statistics are obtained for $k_n/k_0$ and $[V/K]_i/[V/K]_0$ data assuming multiple protons in flight (dashed lines; $y = 2$). Fitting results: (A) $^{D_2O}k_{cat} = 1.5 \pm 0.1$, $y = 2$, $R^2 = 0.98_4$; (B) $^{D_2O}V/K = 2.0 \pm 0.1$, $y = 2$, $R^2 = 0.98_6$).

## RESULTS

**Solvent Kinetic Isotope Effects.** Solvent kinetic isotope effects (SKIE) were used to investigate the rate-limiting chemical steps in CDO catalysis. CDO uses both Cys and $O_2$ as cosubstrates and thus it is critical to first confirm that the atmospheric concentration of oxygen utilized in these experiments (~230 $\mu$M) is sufficient to saturate CDO kinetics. In these experiments, the initial rate of $O_2$ consumption was measured at selected concentrations of Cys and oxygen at pH 8.5 and 37 °C. As shown in the Supporting Information (Figure S1), no difference is observed in the apparent steady-state kinetic parameters ($k_{cat}$ and $K_M$) determined at oxygen concentrations fixed between 50−230 $\mu$M. Since the steady-state curves obtained overlap within this range, CDO must be fully saturated in oxygen even at the lowest concentration utilized (50 $\mu$M). This implies that the apparent $K_M^{O_2}$ must be significantly lower (~10×) than the lowest value of oxygen used. Thus, despite not being able to directly measure the apparent $K_M^{O_2}$ for CDO, this confirms that enzyme is fully saturated at atmospheric oxygen concentrations.[39]

The effect of $D_2O$ on the pH dependence of $k_{cat}$ and $k_{cat}/K_M$ for CDO was measured over the accessible pH range of the enzyme ($6 < pL < 9$). Shown in Figure 2 is the effect of $D_2O$ on the $k_{cat}$ (A, circles) and $k_{cat}/K_M$ (B, squares) pH/D profile obtained from the initial rate of CSA formation. For all pL profiles shown in Figure 2, the $\log(k_{cat})$ and $\log(k_{cat}/K_M)$ data begin at a limiting minimum value and then increase to a maximum limiting value at elevated pH/D. All data were fit to eq 1 (solid lines) by the least-squares method to obtain the observed $pK_a$ for ionizable groups involved in catalysis. From this analysis, a $pK_a$ value (7.4 ± 0.1) was obtained from the $k_{cat}$−pH profile in $H_2O$ reactions at 20 °C (○). The limiting values $Y_H$ and $Y_L$ for CDO $k_{cat}$ over this profile were 0.60 ± 0.04 and 0.17 ± 0.01 $s^{-1}$, respectively. Relative to $H_2O$ reactions, the observed $k_{cat}$ decreases slightly for CDO assays carried out in $D_2O$ (●). The $k_{cat}$ values obtained in $D_2O$ reactions varied between limits $Y_H$ (0.39 ± 0.02 $s^{-1}$) and $Y_L$ (0.13 ± 0.01 $s^{-1}$). Additionally, the $pK_a$ value determined from the $k_{cat}$−pD profile increases to 7.6 ± 0.1 ($\Delta pK_a \sim 0.2$). The upward shift in the $pK_a$ observed in $D_2O$ as compared to that in $H_2O$ is consistent with what is typically observed for ionizable groups involved in catalysis.[40,41] By contrast, the $pK_a$ values obtained from $k_{cat}/K_M$−pL data fits in $H_2O$ (7.9 ± 0.2) show no significant deviation from data obtained in $D_2O$ (7.8 ± 0.1). The absence of any detectible shift in the observed $pK_a$ in $H_2O$ compared to that in $D_2O$ is consistent with what has been described for reactions involving metal-bound waters.[37,40,41] The limiting values obtained from analysis of $k_{cat}/K_M$−pH data were $Y_L$ (67 ± 7 $M^{-1}$ $s^{-1}$) and $Y_H$ (230 ± 18 $M^{-1}$ $s^{-1}$). By comparison, $k_{cat}/K_M$ values decrease to $Y_L$ (28 ± 3 $M^{-1}$ $s^{-1}$) and $Y_H$ (113 ± 10 $M^{-1}$ $s^{-1}$) in $D_2O$ reactions.

The observed solvent isotope effect (SKIE) for each kinetic parameter ($k_{cat}$ and $k_{cat}/K_M$) can be determined from the pH-independent regions of each curve. Within the basic plateau of the $k_{cat}$−pL profile (Figure 2A), a SKIE of 1.45 ± 0.05 is obtained for CDO catalysis. This value is not significantly deviant from the relative viscosity difference between a $D_2O$ solution and water. Additional viscosity experiments are presented below to specifically address if attenuation of $k_{cat}$ and $k_{cat}/K_M$ is due to increased viscosity. By comparison, the solvent isotope effect on the $k_{cat}/K_M$−pH profile is significantly more pronounced within the basic branch of the curve (SKIE of is 2.0 ± 0.1).

**Proton Inventories.** Proton inventory experiments were performed to provide greater insight into the observed solvent isotope effects for CDO-catalyzed CSA formation. In these experiments, the kinetic parameters are determined in various mixtures of $H_2O$ and $D_2O$ within the pH-independent regime of each pL profile. As demonstrated in Figure 2, both $k_{cat}$ and $k_{cat}/K_M$ values are pH-independent at pL 8.5; thus, proton inventory experiments were performed at this pL (8.5). Figure 3 illustrates the relative change in $k_{cat}$ ($k_n/k_0$, A) and $k_{cat}/K_M$ ($[V/K]_n/[V/K]_0$, B) as a function of $D_2O$ mole fraction ($n$). For each data set, the SKIE determined experimentally from $k_{cat}$−pL and $k_{cat}/K_M$−pL profiles (1.45 ± 0.05 and 2.0 ± 0.1, respectively) were used in eq 2 to fit results. At first glance, the $k_{cat}$−proton inventory data appear to be fairly linear, suggesting a single proton in flight. However, the data obtained could not be fit using the solvent isotope effect determined from $k_{cat}$−pL experiments with a single proton model (solid line; eq 2, $y = 1$). Significantly better agreement was obtained by fitting to a multiple proton model (dashed line; eq 2, $y = 2$, $R^2 = 0.98_4$). This suggests that more than one proton-sensitive transition state exists following $O_2$ activation by the enzyme−substrate complex.

By contrast, the concave upward curvature of the $k_{cat}/K_M$−proton inventory is more readily apparent than for $k_{cat}$−proton inventory. This indicates that more than one proton-sensitive transition state exists leading to $O_2$ activation. Reasonable fits were obtained assuming a multiple proton model (dashed line;


dx.doi.org/10.1021/bi501241d | Biochemistry 2014, 53, 7541−7548

eq 2, $y = 2$, $R^2 = 0.98_6$) and a solvent inventory effect on $k_{cat}/K_M$ of 2.0 ± 0.1. For comparison, the single proton fit is illustrated by the solid line.

**Influence of Solvent Isotope Effects on Enzymatic Coupling.** Proton inventory experiments were also performed to evaluate the effect on productive catalysis at pL 8.5. In these experiments, the coupling values obtained at each mole fraction $D_2O$ ($^nC$) were normalized for the coupling observed in $H_2O$ reactions ($^HC$). In the absence of $D_2O$, the initial rate of CSA formation over $O_2$ consumption is $^HC = 0.76 \pm 0.04$. This value agrees fairly well with what has been previously reported for the wild-type enzyme.[21] Remarkably, as shown in Figure 4, the

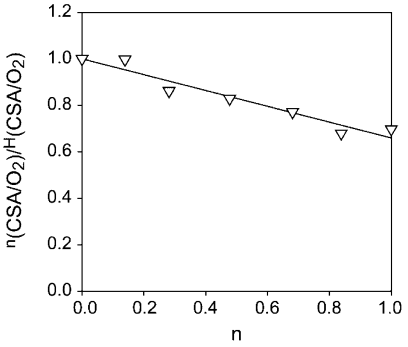


**Figure 4.** Proton inventory for CDO enzymatic coupling (CSA produced per $O_2$ consumed) at pL 8.5. Data were fit to eq 3 with a normal solvent isotope effect in $D_2O$ of 1.45 ± 0.02.

normalized coupling of CDO ($^nC/^HC$) decreases linearly with increasing mole fraction $D_2O$. Coupling data were fit to eq 3, yielding a straight line with a solvent isotope effect in 100% $D_2O$ reactions of 1.45 ± 0.02 on productive catalysis. The linear dependence is consistent with a single proton in flight in the transition state following formation of the (substrate/oxygen)-bound enzyme complex.

**Viscosity Effects.** The effect of solvent viscosity on $k_{cat}$ and $k_{cat}/K_M$ was measured to evaluate the degree to which diffusion into and out of the active site influences the rate of steady-state catalysis. As with proton inventory experiments, these measurements were made within the pH-independent region at pH 8.5. Shown in Figure 5 is the observed $k_{cat}$ value obtained in the absence of viscosigen ($k_0$) normalized for the value obtained at selected relative viscosities ($k_n$). Experiments were performed using two separate viscosigens, glycerol (○) and sucrose (●), and the results were fit to eq 4. The dashed lines in Figure 5 represent the theoretical limits of this experiment. A positive slope of 1.0 is expected if catalysis is entirely diffusion-limited by non-chemical steps in catalysis. Alternatively, the horizontal dashed line represents the expected result assuming no diffusional limitation whatsoever.[33] In practice, the impact of solvent viscosity on $k_{cat}$ should be independent of viscosigen; therefore, the increased viscosity effect observed for reactions carried out in glycerol ($m = 0.38 \pm 0.03$) as compared to those in sucrose ($m = 0.17 \pm 0.02$) suggests an interaction between CDO and glycerol. This could potentially be attributed to promiscuous binding of glycerol within the active site or a perturbation to the enzymatic tertiary structure. Regardless, glycerol clearly has a negative influence on enzymatic activity beyond the simple increase in solvent viscosity. The influence of solvent viscosity on $k_{cat}/K_M$ was also monitored for comparison. In these experiments, only sucrose was used to adjust viscosity. As illustrated in Figure 5, solvent viscosity

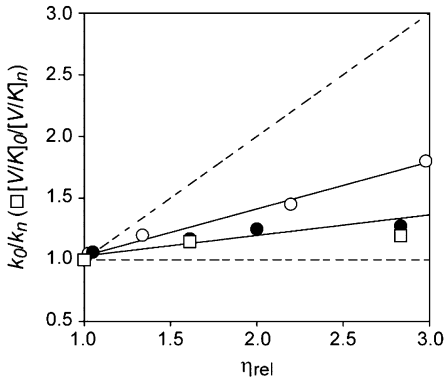


**Figure 5.** Effect of solvent viscosity on the maximal rate ($v_0/[E]$) of CDO-catalyzed CSA formation at pH 8.5. Solvent viscosity was adjusted by increasing concentration of sucrose (●) and glycerol (○). The effect of solvent viscosity on $k_{cat}$ ($k_0/k_n$) and $k_{cat}/K_M$ $(V/K]_0/[V/K]_n$) is designated by circles (black and white) and squares (gray), respectively. The dashed lines represent the theoretical limits for diffusion-limited product release.

effects on $k_{cat}$ and $k_{cat}/K_M$ are significantly below what is predicted for diffusion-limited non-chemical steps. Thus, CDO catalysis is only partially limited by product release and/or substrate binding.

## DISCUSSION

To date, cysteine dioxygenase has been the focus of numerous spectroscopic and crystallographic studies. Despite its extensive characterization, almost nothing is known regarding the timing of catalytic events within the kinetic mechanism of this enzyme. The experiments presented here establish that multiple solvent-exchangeable protons are involved in the CDO-catalyzed formation of CSA. Over the experimental pH range (6–9), the $k_{cat}$–pH profiles exhibited a single p$K_a$, 7.4 ± 0.1. As expected for the ionization of a weak acid, the observed p$K_a$ within $D_2O$ reactions increases to 7.6 ± 0.1.[42] The $\Delta pK_a$ of ~0.2 units are quite similar to what has been reported previously for cysteine sulfhydryl groups.[37,40] Nonetheless, the identity of this ionizable group cannot be unambiguously identified on the basis of the $\Delta pK_a$ value alone. The $k_{cat}$–pL profile is primarily a reflection of the irreversible processes following formation of the ($O_2$/Cys)-bound enzyme complex. Therefore, the solvent isotope effect observed on $k_{cat}$ (1.45 ± 0.05) could suggest a rate-limiting chemical step or product release. This conclusion is supported by proton inventory results for $k_{cat}$ shown in Figure 3, suggesting that more than one proton-sensitive transition state is present following $O_2$ activation by the enzyme–substrate complex.

Complementary proton inventory ($O_2$/CSA)-coupling experiments were performed to better understand the nature of the proton-sensitive step(s) observed for $k_{cat}$ data. General treatments for isotope effects on the partitioning parallel reaction pathways among $O_2$-dependent monooxygenases (P450, tyrosine hydroxylase) have been described at length elsewhere.[38,43] A significant advantage of these experiments is that the solvent isotope effect on coupling CSA formation and $O_2$ consumption is solely a function of the partitioning between the productive and unproductive catalytic branches and therefore the data is independent of substrate binding and/or product release.[38] Further discussion of this kinetic model and the derivation of kinetic expressions can be found in Supporting Information. Figure 4 illustrates the influence of $D_2O$ on the


dx.doi.org/10.1021/bi501241d | Biochemistry 2014, 53, 7541–7548

ratio of $O_2$ consumed per mol of CSA produced. In the absence of $D_2O$, typical coupling ($^{H}C$) for CDO is ~76 ± 4%, where as in pure $D_2O$, this value ($^{D}C$) decreases to 53 ± 4%. The linear proton inventory of the normalized coupling is well fit to eq 3, yielding a straight line and a solvent isotope effect in 100% $D_2O$ reactions of 1.45 ± 0.02. This solvent isotope effect is consistent with the values obtained from both $k_{cat}$–pL profile and $k_{cat}$ proton inventory experiments. Since the coupling proton inventories reflect only the partitioning between productive and unproductive steps, the linear dependence of this data indicates a single proton-sensitive transition state within the productive catalytic branch. Since proton inventory on $k_{cat}$ data (Figure 3A) indicates multiple protons in flight, at least one additional rate-limiting protonation event must occur beyond the Cys oxidation step. Presumably, this could occur during product release. As noted in the Supporting Information, eq 3 is used to describe the expected proton inventory for an isotope-sensitive transition state within the productive reaction path. Alternative expressions can be derived for systems with a proton-sensitive transition state in the unproductive reaction pathway (equation S7). No reasonable fits could be obtained by fitting proton inventory to this alternative kinetic model.

Within the same pH range, the $k_{cat}/K_M$–pH profile also exhibits a single p$K_a$ (7.9 ± 0.1), although this value is slightly higher than that observed in $k_{cat}$–pH profile. Furthermore, no significant shift in the p$K_a$ is observed in $D_2O$ reactions within the $k_{cat}/K_M$–pD profile. This is consistent with the involvement of a metal-bound solvent molecule(s) in the reaction mechanism leading to the first irreversible step.[37,40] Furthermore, proton inventory experiments on $k_{cat}/K_M$ indicate that more than one proton-sensitive transition state exists leading to $O_2$ activation. The increased magnitude of solvent isotope effects observed for $k_{cat}/K_M$ data (relative to $k_{cat}$) would seem to suggest that solvent plays a greater role in the initial reversible steps up to $O_2$ binding. This could potentially reflect initial displacement of Fe-bound solvent molecules during substrate binding. This would also explain the absence of a Δp$K_a$ observed in $k_{cat}/K_M$–pL data.

For diffusion-controlled reactions in which product release is rate-limiting, $k_{cat}$ would be attenuated by increased solvent viscosity. Addition of $D_2O$ to reaction buffers increases the relative viscosity of reaction mixtures, giving rise to an apparent solvent isotope effect. Thus, the small isotope effect observed in $k_{cat}$–pL profiles (1.45 ± 0.05) may simply be due to increased viscosity. However, the viscosity experiments performed clearly demonstrate that this is not the case. The relative viscosity of $D_2O$ ($\eta_{rel}$ ~ 1.24) is closely matched by experiments performed in 9% (w/w) glycerol.[34,44] From the viscosity experiments performed, the expected attenuation of $k_{cat}$ at this viscosity would be 6–12% within sucrose and glycerol (1.12 ± 0.04). Therefore, viscosity effects do not significantly contribute to the solvent isotope effect observed in the $k_{cat}$–pL profile. As solvent viscosity imparts no significant perturbation to $k_{cat}/K_M$ results, the same argument can be made for solvent isotope effects observed within the $k_{cat}/K_M$–pL profile. Taken together, the viscosity studies presented here indicate that the non-chemical steps in CDO catalysis (product release and/or substrate binding) are only partially limited by diffusion and do not significantly contribute to observed isotope effects on $k_{cat}$ or $k_{cat}/K_M$.

On the basis of the collected experiments presented here, a kinetic mechanism for CDO-catalyzed Cys oxidation is shown in Scheme 1. The high-resolution crystal structure for resting CDO [**E**] (PDB code 4IEZ) at pH 8 identifies 2 Fe-bound

**Scheme 1. Proposed Kinetic Model for CDO-Catalyzed Reaction**

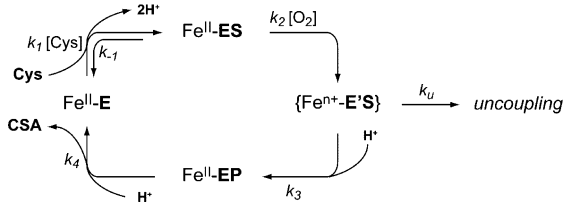


solvent molecules (OH or $H_2O$) in the absence of substrate.[10] If the positive charged R60 guanidinium group is taken into consideration, then coordination of the active site ferrous iron by 3 neutral His residues leaves three positive charges unaccounted for within the CDO active site. Hydrogen bonding between E104 and H140 can compensate for one of these positive charges, and inclusion of two hydroxide anions as the bound solvent molecules would provide overall charge neutrality to the active site (Figure 1A). Substrate binding of Cys to the Fe site requires deprotonation of substrate thiol and amine functional groups. On the basis of mass balance, substrate binding should release 2 protons from the active site. Protonation of the Fe-bound hydroxides by incoming Cys substrate would yield more labile $H_2O$ ligands and maintain the overall charge neutrality within the active site (Figure 1B). Furthermore, the involvement of 2 metal bound solvent molecules in the initial steps up to $O_2$ bindng agrees well with conclusions made on the basis of $k_{cat}/K_M$–pL and $k_{cat}/K_M$–proton inventory data.

It could also be argued that the p$K_a$ values observed in $k_{cat}$ and $k_{cat}/K_M$ results could be attributed to the ionization of key active site residues within the CDO active site. For instance, both Y157 and H155 are conserved in CDO enzymes across phylogenic domains. As activity increases with pH, a general base mechanism could be considered utilizing either residue. However, the absence of a shift in the $k_{cat}/K_M$–p$K_a$ value obtained in $D_2O$ relative to that in $H_2O$ is inconsistent with the well-established ionization behavior typical of general acid/base chemistry.[42] This behavior is more consistent with what has been reported for metal-bound ionizable groups.[37,40] Thus, although we cannot unambiguously state that the rate-limiting ionization steps are solely due to substrate-binding, this model represents the simplest explanation for all experimental behavior.

In the context of reactions performed at atmospheric oxygen concentration, the independence of steady-state kinetic parameters $k_{cat}$ and $K_M$ observed for reactions at fixed oxygen concentrations ranging 50–230 μM suggests that the apparent $K_M^{O_2}$ must be substantially lower (~10×) than the lowest value of oxygen used.[39] Therefore, the binding of $O_2$ to the substrate-bound enzyme complex [**ES**] to produce the substrate-oxidizing ternary complex [**E′S**] can be treated as an irreversible process. At this point in the kinetic mechanism, the reaction can partition to either the productive ($k_3$) or unproductive ($k_u$) reaction pathways. Proton inventory experiments suggest two proton-sensitive steps following irreversible $O_2$ binding. Most importantly, a solvent isotope effect on ($O_2$/CSA) coupling suggests a single proton-sensitive transition state within the productive catalytic pathway. This observation


dx.doi.org/10.1021/bi501241d | Biochemistry 2014, 53, 7541–7548

may indicate that protonation of a transient iron−oxo intermediate ($Fe^{III}$−superoxide or $Fe^{IV}$−peroxo) precedes formation of the substrate-oxidizing species. Indeed, similar behavior has been reported in biologically inspired non-heme iron catalysts.[45] As unproductive catalysis is expected to produce reactive oxygen species ($O_2^{\bullet-}$ or $O_2^{2-}$), it is not clear from initial rate experiments if the enzyme release from this uncoupled pathway retains activity. The release of oxidized catalytically inactive $Fe^{III}$−CDO seems to be very likely. Since Cys is also a reductant, excess substrate may be able to rescue enzymatic activity, providing no degradation of the enzyme itself.

## ■ ASSOCIATED CONTENT

### Supporting Information

Steady-state kinetic parameters ($k_{cat}$ and $K_M$) determined at fixed oxygen concentrations and a detailed description of coupling proton inventory expressions and equations. This material is available free of charge via the Internet at http://pubs.acs.org.

## ■ AUTHOR INFORMATION


### Corresponding Author

*Phone: (817) 272-9066. Fax: (817) 272-3808. E-mail: bspierce@uta.edu.



### Funding

This work was supported by NSF (CHE) 1213655 and The University of Texas at Arlington, Research Enhancement Award (acct. no. 14-7488-74) awarded to B.S.P.


### Notes

The authors declare no competing financial interest.

## ■ ACKNOWLEDGMENTS


We would like to thank Paul Fitzpatrick (UT Health Science Center, San Antonio, TX) for his assistance and useful conversations.


## ■ ABBREVIATIONS

CDO, cysteine dioxygenase; Cys, cysteine; CSA, cysteine sulfinic acid; HPLC, high-performance liquid chromatography; KIE, kinetic isotope effect

## ■ REFERENCES


(1) Dominy, J. E., Simmons, C. R., Hirschberger, L. L., Hwang, J., Coloso, R. M., and Stipanuk, M. H. (2007) Discovery and characterization of a second mammalian thiol dioxygenase, cysteamine dioxygenase. *J. Biol. Chem. 282*, 25189−25198.

(2) Stipanuk, M., Simmons, C., Andrew Karplus, P., and Dominy, J., Jr. (2011) Thiol dioxygenases: unique families of cupin proteins. *Amino Acids 41*, 91−102.

(3) Reddie, K. G., and Carroll, K. S. (2008) Expanding the functional diversity of proteins through cysteine oxidation. *Curr. Opin. Chem. Biol. 12*, 746−754.

(4) Winyard, P. G., Moody, C. J., and Jacob, C. (2005) Oxidative activation of antioxidant defence. *Trends Biochem. Sci. 30*, 453−461.

(5) Trachootham, D., Alexandre, J., and Huang, P. (2009) Targeting cancer cells by ROS-mediated mechanisms: a radical therapeutic approach? *Nat. Rev. Drug Discovery 8*, 579−591.

(6) Behave, D. P., Muse, W. B., and Carroll, K. S. (2007) Drug targets in mycobacterial sulfur metabolism. *Infect. Disord.: Drug Targets 7*, 140−158.

(7) Costas, M., Mehn, M. P., Jensen, M. P., and Que, L. (2004) Dioxygen activation at mononuclear nonheme iron active sites: enzymes, models, and intermediates. *Chem. Rev. 104*, 939−986.

(8) Ye, S., Wu, X. a., Wei, L., Tang, D., Sun, P., Bartlam, M., and Rao, Z. (2007) An insight into the mechanism of human cysteine dioxygenase: key roles of the thioether-bonded tyrosine−cysteine cofactor. *J. Biol. Chem. 282*, 3391−3402.

(9) McCoy, J. G., Bailey, L. J., Bitto, E., Bingman, C. A., Aceti, D. J., Fox, B. G., and Phillips, G. N., Jr. (2006) Structure and mechanism of mouse cysteine dioxygenase. *Proc. Natl. Acad. Sci. U.S.A. 103*, 3084−3089.

(10) Driggers, C. M., Cooley, R. B., Sankaran, B., Hirschberger, L. L., Stipanuk, M. H., and Karplus, P. A. (2013) Cysteine dioxygenase structures from pH 4 to 9: consistent Cys−persulfenate formation at intermediate pH and a Cys-bound enzyme at higher pH. *Mol. Microbiol. 425*, 3121−3136.

(11) Straganz, G. D., and Nidetzky, B. (2006) Variations of the 2-His-1-carboxylate theme in mononuclear non-heme Fe(II) enzymes. *ChemBioChem. 7*, 1536−1548.

(12) Straganz, G. D., Diebold, A. R., Egger, S., Nidetzky, B., and Solomon, E. I. (2010) Kinetic and CD/MCD spectroscopic studies of the atypical, three-His-ligated, non-heme $Fe^{2+}$ center in diketone dioxygenase: the role of hydrophilic outer shell residues in catalysis. *Biochemistry 49*, 996−1004.

(13) Adams, M. A., Singh, V. K., Keller, B. O., and Jia, Z. (2006) Structural and biochemical characterization of gentisate 1,2-dioxygenase from *Escherichia coli* O157:H7. *J. Mol. Biol. 61*, 1469−1484.

(14) Koehntop, K., Marimanikkuppam, S., Ryle, M., Hausinger, R., and Que, L. (2006) Self-hydroxylation of taurine/alpha-ketoglutarate dioxygenase: evidence for more than one oxygen activation mechanism. *J. Biol. Inorg. Chem. 11*, 63−72.

(15) Ryle, M. J., Koehntop, K. D., Liu, A., Que, L., and Hausinger, R. P. (2003) Interconversion of two oxidized forms of taurine/α-ketoglutarate dioxygenase, a non-heme iron hydroxylase: evidence for bicarbonate binding. *Proc. Natl. Acad. Sci. U.S.A. 100*, 3790−3795.

(16) Ge, Y., Lawhorn, B. G., El Naggar, M., Sze, S. K., Begley, T. P., and McLafferty, F. W. (2003) Detection of four oxidation sites in viral prolyl-4-hydroxylase by top-down mass spectrometry. *Protein Sci. 12*, 2320−2326.

(17) Farquhar, E. R., Koehntop, K. D., Emerson, J. P., and Que, L., Jr. (2005) Post-translational self-hydroxylation: a probe for oxygen activation mechanisms in non-heme iron enzymes. *Biochem. Biophys. Res. Commun. 338*, 230−239.

(18) Myllylä, R., Majamaa, K., Günzler, V., Hanauske-Abel, H. M., and Kivirikko, K. I. (1984) Ascorbate is consumed stoichiometrically in the uncoupled reactions catalyzed by prolyl 4-hydroxylase and lysyl hydroxylase. *J. Biol. Chem. 259*, 5403−5405.

(19) Dominy, J. E., Jr., Hwang, J., Guo, S., Hirschberger, L. L., Zhang, S., and Stipanuk, M. H. (2008) Synthesis of amino acid cofactor in cysteine dioxygenase is regulated by substrate and represents a novel post-translational regulation of activity. *J. Biol. Chem. 283*, 12188−12201.

(20) Siakkou, E., Rutledge, M. T., Wilbanks, S. M., and Jameson, G. N. L. (2011) Correlating crosslink formation with enzymatic activity in cysteine dioxygenase. *Biochim. Biophys. Acta 1814*, 2003−2009.

(21) Li, W., Blaesi, E. J., Pecore, M. D., Crowell, J. K., and Pierce, B. S. (2013) Second-sphere interactions between the C93−Y157 cross-link and the substrate-bound Fe site influence the $O_2$-coupling efficiency in mouse cysteine dioxygenase. *Biochemistry 52*, 9104−9119.

(22) Tchesnokov, E. P., Wilbanks, S. M., and Jameson, G. N. L. (2011) A strongly bound high-spin iron(II) coordinates cysteine and homocysteine in cysteine dioxygenase. *Biochemistry 51*, 257−264.

(23) Blaesi, E. J., Fox, B. G., and Brunold, T. C. (2014) Spectroscopic and computational investigation of iron(III) cysteine dioxygenase: implications for the nature of the putative superoxo-Fe(III) intermediate. *Biochemistry 53*, 5759−5770.

(24) Gardner, J. D., Pierce, B. S., Fox, B. G., and Brunold, T. C. (2010) Spectroscopic and computational characterization of substrate-bound mouse cysteine dioxygenase: nature of the ferrous and ferric cysteine adducts and mechanistic implications. *Biochemistry 49*, 6033−6041.

(25) Pierce, B. S., Gardner, J. D., Bailey, L. J., Brunold, T. C., and Fox, B. G. (2007) Characterization of the nitrosyl adduct of substrate-bound mouse cysteine dioxygenase by electron paramagnetic resonance: electronic structure of the active site and mechanistic implications. *Biochemistry 46*, 8569−8578.
(26) Kumar, D., Thiel, W., and de Visser, S. P. (2011) Theoretical study on the mechanism of the oxygen activation process in cysteine dioxygenase enzymes. *J. Am. Chem. Soc. 133*, 3869−3882.
(27) de Visser, S. P., and Straganz, G. D. (2009) Why do cysteine dioxygenase enzymes contain a 3-His ligand motif rather than a 2His/1Asp motif like most nonheme dioxygenases? *J. Phys. Chem. A 113*, 1835−1846.
(28) Crawford, J. A., Li, W., and Pierce, B. S. (2011) Single turnover of substrate-bound ferric cysteine dioxygenase with superoxide anion: enzymatic reactivation, product formation, and a transient intermediate. *Biochemistry 50*, 10241−10253.
(29) Mirica, L. M., and Klinman, J. P. (2008) The nature of $O_2$ activation by the ethylene-forming enzyme 1-aminocyclopropane-1-carboxylic acid oxidase. *Proc. Natl. Acad. Sci. U.S.A. 105*, 1814−1819.
(30) Hangasky, J. A., Saban, E., and Knapp, M. J. (2013) Inverse solvent isotope effects arising from substrate triggering in the factor inhibiting hypoxia inducible factor. *Biochemistry 52*, 1594−1602.
(31) Price, J. C., Barr, E. W., Hoffart, L. M., Krebs, C., and Bollinger, J. M. (2005) Kinetic dissection of the catalytic mechanism of taurine:α-ketoglutarate dioxygenase (TauD) from *Escherichia coli*. *Biochemistry 44*, 8138−8147.
(32) Glasoe, P. K., and Long, F. A. (1960) Use of glass electrodes to measure acidities in deuterium oxide. *J. Phys. Chem. 64*, 188−190.
(33) Gadda, G., and Fitzpatrick, P. F. (2013) Solvent isotope and viscosity effects on the steady-state kinetics of the flavoprotein nitroalkane oxidase. *FEBS Lett. 587*, 2785−2789.
(34) Henderson Pozzi, M., and Fitzpatrick, P. F. (2010) A lysine conserved in the monoamine oxidase family is involved in oxidation of the reduced flavin in mouse polyamine oxidase. *Arch. Biochem. Biophys. 498*, 83−88.
(35) Denu, J. M., and Fitzpatrick, P. F. (1994) pH and kinetic isotope effects on the oxidative half-reaction of D-amino-acid oxidase. *J. Biol. Chem. 269*, 15054−15059.
(36) Cleland, W. W., and Daniel, L. P. (1982) The use of pH studies to determine chemical mechanisms of enzyme-catalyzed reactions. *Methods Enzymol. 87*, 390−405.
(37) Schowen, K. B., Schowen, R. L., and Daniel, L. P. (1982) Solvent isotope effects on enzyme systems. *Methods Enzymol. 87*, 551−606.
(38) Frantom, P. A., and Fitzpatrick, P. F. (2003) Uncoupled forms of tyrosine hydroxylase unmask kinetic isotope effects on chemical steps. *J. Am. Chem. Soc. 125*, 16190−16191.
(39) Smitherman, C., and Gadda, G. (2013) Evidence for a transient peroxynitro acid in the reaction catalyzed by nitronate monooxygenase with propionate 3-nitronate. *Biochemistry 52*, 2694−2704.
(40) Quinn, D. M., and Sutton, L. D. (1991) Theoretical basis and mechanistic utility of solvent isotope effects, in *Enzyme Mechanism from Isotope Effects* (Cook, P. F., Ed.) pp 73−126, CRC Press, Boca Raton, FL.
(41) Venkatasubban, K. S., and Schowen, R. L. (1984) The proton inventory technique. *Crit. Rev. Biochem. Mol. Biol. 17*, 1−44.
(42) Cleland, W. W. (2003) The use of isotope effects to determine enzyme mechanisms. *J. Biol. Chem. 278*, 51975−51984.
(43) Fitzpatrick, P. F. (1991) Studies of the rate-limiting step in the tyrosine hydroxylase reaction: alternate substrates, solvent isotope effects, and transition-state analogs. *Biochemistry 30*, 6386−6391.
(44) Robbins, J. M., and Ellis, H. R. (2013) Steady-state kinetic isotope effects support a complex role of Arg226 in the proposed desulfonation mechanism of alkanesulfonate monooxygenase. *Biochemistry 53*, 161−168.
(45) Oloo, W. N., Fielding, A. J., and Que, L. (2013) Rate-determining water-assisted O−O bond cleavage of an FeIII−OOH intermediate in a bio-inspired nonheme iron-catalyzed oxidation. *J. Am. Chem. Soc. 135*, 6438−6441.